Hindawi
International Journal of Antennas and Propagation
Volume 2024, Article ID 3452375, 9 pages
https://doi.org/10.1155/2024/3452375

Research Article

Design of a Low Sidelobe Feed Network Based on the Louver-Shaped Defected Ground Structure

Yuan Zhang[1] **and Songtao Xi**[2]

[1]*Nanjing Vocational College of Information Technology, Nanjing 210046, China*
[2]*Nanjing Glarun Defense System Co., Ltd., Nanjing 210039, China*

Correspondence should be addressed to Yuan Zhang; zhangyuan.dz@njcit.cn

Received 25 September 2023; Revised 17 February 2024; Accepted 27 February 2024; Published 25 March 2024

Academic Editor: Rajkishor Kumar

In this paper, a low sidelobe feeding network has been developed utilizing the louver-shaped defected ground structure (DGS). By adjusting the louver-shaped DGS, the output amplitude and phase of the corresponding ports can be altered, minimizing deviations from theoretical values. This enables antenna arrays equipped with this feeding network to more easily achieve low sidelobe performance. The impact of the louver-shaped DGS on the amplitude and phase of each port in the power divider within the feeding network is analyzed, and a 16-channel feeding network incorporating the louver-shaped DGS has been designed, fabricated, and then measured. The test results indicate that the performance of the line-feeding network is effectively improved by designing and adjusting the louver-shaped DGS. Through the debugging procedure, the amplitude deviation of the feeding network has been reduced from ±0.45 dB to ±0.2 dB, while the phase deviation of the feeding network has been reduced from ±8° to ±2.5°, and the maximum value of the first sidelobe has been reduced from −24.2 dB to −28.1 dB.

1. Introduction

The reduction in size and portability of communication equipment has led to an increased emphasis on antenna miniaturization in wireless communication systems [1]. Verma et al. [2] have proposed using a miniaturized artificial magnetic conductor (AMC) to improve the bandwidth and gain of the PIFA antenna, while reducing the occupied area of the antenna. A systematic feeding network is necessary to drive multiple antenna elements, and the complexity of this network has grown due to the large number of elements. Due to the limitations of special spatial environments, the design of the feeding network is crucial to meet the electrical performance requirements of the antenna [3].

Multiple row feeds or column feeds are present in the planar array antenna. To achieve low sidelobe or ultralow sidelobe performance of array antennas, the design of the feeding network is very critical, in addition to the performance of the antenna unit itself [4]. Wu et al. [5] propose a 140 GHz high-efficiency slotted waveguide antenna with a low-loss feeding network. Mneesy et al. [6] present the design and implementation of a 60 GHz single-element monopole antenna as well as a two-element array made of two 60 GHz monopole antennas.

The feeding network is typically a multi-channel parallel feeding network that meets specific amplitude and phase weighting requirements. It can be implemented in various forms, such as air-dielectric striplines, microstrip lines, dielectric striplines, and waveguides. Verma and Raghava [7] propose a dual-port multi-input multi-output (MIMO) substrate integrated waveguide (SIW) antenna based on electromagnetic band gap (EBG) technology. Rao et al. [8] introduce a novel MIMO antenna design using the defective ground structure with microstrip line-feeding network as the feeding mechanism.

Due to the small space occupied by dielectric stripline circuits, they are commonly used in microwave multistack structures [9]. The dielectric stripline is generally used in microwave multilayer board design. However, once the laminating process is finished, debugging becomes virtually

impossible. Consequently, the performance of the feeding network is primarily dependent on the initial simulation design and the management of the dielectric plate and processing technology. This includes factors like the dielectric plate's thickness error, dielectric constant error, printed board line width error during processing, and thickness error control during lamination. Nevertheless, errors are inevitable and can impact the accuracy of the amplitude and phase of the feeding network to a certain degree. This impact becomes more pronounced when the feeding network is large and has amplitude and phase weighting. The variation of a single parameter can influence the sidelobe index of the antenna, thereby affecting the amplitude and phase distribution of the entire feeding network.

In this paper, a quantitative method for adjusting the amplitude and phase of the feeding network by etching the louver-shaped defected ground structure (DGS) is provided. In cases where there is a disparity between the actual performance of the feeding network and the theoretical calculations, adjustments to the amplitude and phase can be made by debugging the louver-shaped DGS. This ensures that the final amplitude and phase adhere to the design specifications.

Based on the conventional design, the feeding network added the louver type DGS. This addition allows for the correction of amplitude and phase errors in the power divider of the feeding network by leveraging the slow-wave characteristics of the defect ground. This helps reduce the amplitude and phase error caused by changes in plate thickness and dielectric constant of the feeding network.

With the rapid development of radar, satellite communication and other fields, the demand for low sidelobe is increasing. Lower sidelobe levels can ensure the effective operation of the system, and a lower sidelobe level represents a smaller impact on other systems. Especially in the context of the comprehensive application of multiple systems, low sidelobe technology is receiving increasing attention.

Table 1 presents the recently developed low sidelobe technique, which is compared with the louver type DGS feeding technique. It provides a series-parallel method to weigh the amplitude of the acoustic array elements of a 15-element linear array to achieve low sidelobe levels in the linear array [10]. The theoretical maximum sidelobe for this linear array is −23.0 dB at 80 kHz. In testing the sample array in an anechoic water tank, the measured maximum sidelobe has been found to be −19.0 dB. However, a notable disparity exists between the actual measurement and the theoretical estimation. While the paper presents the low sidelobe technique, it does not explicitly address methods to reconcile this particular discrepancy.

In addition, the coefficients of the aperture field distribution function can be optimized by improving the genetic algorithm (GA) [11]. Zhang [12] summarizes the design method for an ultralow sidelobe reflector antenna, which achieves low sidelobes through Taylor amplitude weighting. Simulation results show that the sidelobes are better than −40.0 dB. A tree topology structure is employed in the unequal power division ratio feeding network, meeting the power distribution ratio and phase consistency at the operating frequency of 9.4 GHz, and achieving the first sidelobe of −25 dB at the center frequency from [13].

References [11–13] have presented design simulation results without conducting actual testing and have not compared the consistency between measured and theoretical estimates. However, due to challenges in controlling production consistency such as processing errors and material variations, the physical test values of the feeding network are inevitably going to differ from the theoretical design. In the existing literature, there are few solutions to address these discrepancies. When the amplitude and phase requirements of the actually produced feeding network significantly deviate from theoretical calculations and cannot be corrected through debugging methods, the produced feeding network may need to be discarded or used with reduced requirements.

However, if the feeding network is debugged through the DGS, its performance can be improved to meet usage requirements. The debugged feeding network meets the original requirements and does not need to be scrapped or downgraded, thus eliminating the need for re-production and greatly reducing production costs and cycles. Therefore, the use of this method can minimize discrepancies between design and the solidified production process, address material inconsistencies, and drastically cut down on the time required for repeated design and verification, ultimately leading to reduced production costs and shorter cycles.

2. Defected Ground Structure

Yablonovitch [14] introduce the concept of photonic band gap (PBG), a periodic structure known for providing rejection of certain frequency bands. Park et al. [15] propose a DGS, which is designed by connecting two square PBG cells with a thin slot. The DGS is an etched periodic or nonperiodic cascaded corrosion defect in the ground of various planar transmission lines, such as microstrip, coplanar, and conductor-backed coplanar waveguide [16]. The DGS is noted for its minimal space requirements and straightforward design, achieved by etching a slot in the ground plane of the microstrip circuit. Additionally, Suvarna et al. [17] introduces a new pi-shaped DGS with three annular rings which is etched in the ground plane. Furthermore, Ghaloua et al. [18] propose the utilization of a new geometric DGS on an FR-4 substrate with a relative permittivity equal to 4.4, a thickness of 1.6 mm, and a loss tangent of 0.025 to downsize the antenna arrays.

DGS is implemented by etching different shapes in the ground plane. When DGS is realized with a microstrip antenna, the presence of the etched defect in the ground disrupts the current distribution. The microstrip line incorporating DGS exhibits stop-band characteristics, a slow-wave effect, and high impedance. The etched slot causes a disturbance in the shield current distribution in the ground plane. This disturbance changes the effective dielectric constant distribution of the substrate material. This, in turn, modifies the characteristics of the transmission line, such as the distributed inductance and capacitance of the microstrip

Table 1: Comparison of low sidelobe technologies.

Ref	Low sidelobe technology	The maximum value of the first sidelobe at center frequency	
		Simulation design (dB)	Actual measured value after debugging (dB)
This work	Using the louver type DGS	−24.2	−28.1
[10]	Weighting the amplitude of the elements in the linear array in a series-parallel manner	−23	−19
[11]	Optimizing the coefficients of the aperture field distribution function by improving genetic algorithms (GA)	−40	—
[12]	Using taylor amplitude weighting	−24.1	—
[13]	The feeding network design adopts a tree topology structure	−25	—

line. The equivalent circuit of the microstrip line is a parallel resonant RLC circuit, with the capacitance and inductance values in the circuit being contingent upon the size and area of the defect. When a defect is introduced into the transmission line, it can disturb the current shielding distribution. This interference affects the components of the transmission line, such as the line capacitance and inductance. Therefore, any defects etched in the microstrip line will induce changes in the effective inductance and capacitance of the transmission line.

Figure 1 depicts the dumbbell-shaped DGS module. It consists of two rectangular defected areas, each with dimensions $a \times b$. These two rectangular areas are linked by a slender connecting slot of dimensions $g \times w$. Additionally, there are wide etched areas on the backside of the metallic ground plane.

The dumbbell-shaped DGS is a widely utilized and traditional form of DGS structure. This structure has the advantages such as its simple structure, limited design parameters, single-pole, low-pass characteristics, and ease of analysis and design. It has been extensively employed and researched in the field of microwave circuit design [19].

In the DGS, the electric field is concentrated around the narrow etched gap, while the current is confined to the metallic ground plane surrounding the circular etched pattern at resonance [20]. The rectangular areas of the dumbbell-shaped DGS enhance the effective inductance of the microstrip line, while the connecting slot between these areas improves the effective capacitance of the microstrip line. The two $a \times b$ rectangular defected areas and a connecting slot correspond to added inductance and capacitance, respectively. The RLC resonant circuit model can be utilized to represent the dumbbell-shaped DGS in the ground plane based on the loss, as depicted in Figure 2.

The equivalent circuit parameters can be expressed using the following equations (1)–(4).

$$\omega_0 = \frac{1}{\sqrt{L_p C_p}}, \tag{1}$$

$$C_p = \frac{\omega_c}{2Z_0\left(\omega_0^2 - \omega_c^2\right)}, \tag{2}$$

$$L_p = \frac{1}{4\pi^2 f_0^2 C_p}, \tag{3}$$

$$R(\omega) = \frac{2Z_0}{\sqrt{\left(2/\left|S_{11}(\omega)\right|^2\right) - \left(2Z_0\left(\omega_C - \left(1/\omega_L\right)\right)\right)^2 - 1}}, \tag{4}$$

where f_0 is the resonant frequency, Z_0 is the 50 ohms characteristic impedance of microstrip line, ω_0 is the angular resonant frequency, ω_C is the 3 dB cutoff angular frequency, and $S_{11}(\omega)$ is the input reflection coefficient of the equivalent network. The value of the equivalent inductance L_p depends on the area of the $a \times b$ rectangular defective at both ends of the dumbbell. The larger the area of the square, the greater the value of L_p. The value of the equivalent capacitance C_p depends on the length of w.

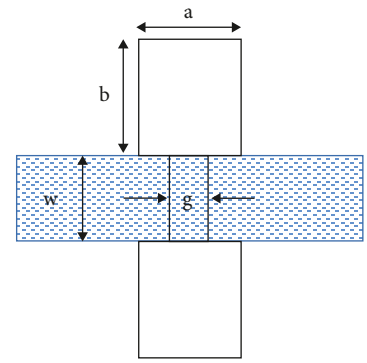

Figure 1: The dumbbell-shaped DGS module.

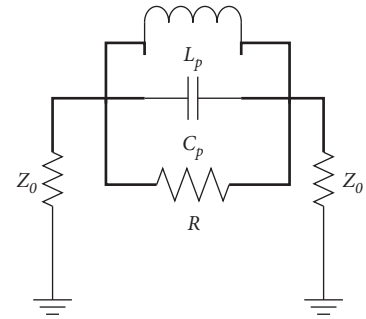

Figure 2: RLC resonant circuit model.

3. Design of the Louver-Shaped DGS

By etching the defect pattern on the grounding plate of the microstrip line, the DGS modifies the distribution inductance and capacitance of the microstrip line. Similarly, etching defects on the grounding plate of the dielectric stripline can also lead to alterations in the distribution of inductance and capacitance within the dielectric stripline.

The relationship between the characteristic impedance (Z) and phase velocity (V_φ) of the stripline and the distributed capacitance (C) and inductance (L) of the stripline can be expressed as follows:

$$Z = \sqrt{\frac{L}{C}}, \tag{5}$$

$$V_\varphi = \frac{1}{\sqrt{LC}}. \tag{6}$$

Consequently, when the distributed inductance (L) or capacitance (C) of the stripline changes, the characteristic impedance (Z) and phase velocity (V_φ) change accordingly [21].

Since only one variable, either the distributed inductance (L) or capacitance (C), needs to be changed, the dumbbell-shaped DGS is transformed into a rectangular-shaped DGS by altering either the area of the $a \times b$ rectangular defect or the size of the width (w).

In cases where the impact of a single defect on the characteristic impedance (Z) and phase velocity (V_φ) is insufficient, the DGS can be cascaded to create a louver-shaped DGS, thereby enhancing the effect.

Figure 3 illustrates the louver-shaped DGS structure, which is positioned just above the transmission lines on the radio frequency ground. These transmission lines are ribbon lines.

Figure 4 depicts the simulation models of transmission lines with the louver-shaped DGS from P3 to P4 and equi-width transmission lines without DGS from P1 to P2.

In this simulation model from P3 to P4, a louver-shaped DGS structure consisting of eight side-by-side rectangular-shaped DGS units is designed. Each defect measures 1 mm × 8 mm, with an interval of 1 mm between them. The transmission line has a width of 1.3 mm, the printed circuit board cavity height is 2 mm, and the dielectric constant is 2.94.

Figure 5 illustrates the difference in impedance between transmission lines equipped with the louver-shaped DGS and those lacking DGS. The simulation results of $Z1$, representing the stripline without DGS, and $Z3$, representing the stripline with the louver-shaped DGS, are shown in Figure 4. The data indicate that the stripline with the louver-shaped DGS exhibits a characteristic impedance of 52.194 Ω, while the stripline without DGS exhibits a characteristic impedance of 51.77 Ω at the central frequency of 1.3 GHz. The addition of the louver-shaped DGS to the stripline results in an increase of approximately 0.4 Ω in the characteristic impedance. This increase is attributed to the augmented effective distributed inductance caused by the louver-shaped DGS.

The difference in phase between transmission lines equipped with the louver-shaped DGS and those without DGS is illustrated in Figure 6. The simulation results of S12, representing the stripline without DGS, and S34, representing the stripline with the louver-shaped DGS, are shown in Figure 6.

The dimensions of the rectangular defected area ($a \times b$) and the length of w of the louver-shaped DGS impact the value of the equivalent capacitance and the equivalent inductance. According to equations (5) and (6), changes in the distributed inductance or capacitance of the stripline lead to corresponding alterations in characteristic impedance and phase velocity. Through simulation experiments, it is observed that the use of a louver-shaped DGS consisting of 8 rectangles resulted in an approximately 4.5-degree increase in the characteristic phase of the stripline at the center frequency of 1.3 GHz. As shown in the figure, the characteristic phase of the stripline with the louver-shaped DGS is 45.28 degrees, while the characteristic phase of the stripline without DGS is 40.83 degrees at this frequency. This indicates that the phase modulation of the louver-shaped DGS increases with the increase in frequency.

4. Design of Unequal Power Divider Using Louver-Shaped DGS

Figure 7 presents an integrated structure for an unequal power divider that utilizes the louver-shaped DGS with a power ratio of $K^2:1$. The relationship between K and the impedance of each transmission line is as follows:

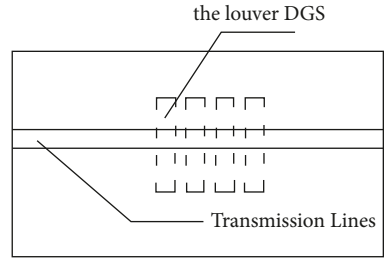

Figure 3: Layout of transmission lines with the louver-shaped DGS model.

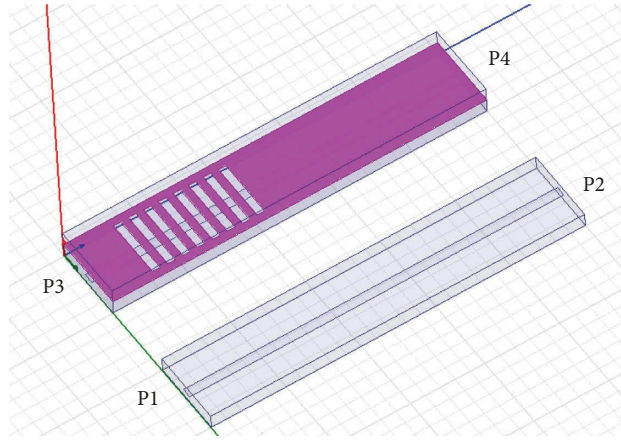

Figure 4: The simulation models of transmission lines with the louver-shaped DGS and equi-width transmission lines without DGS.

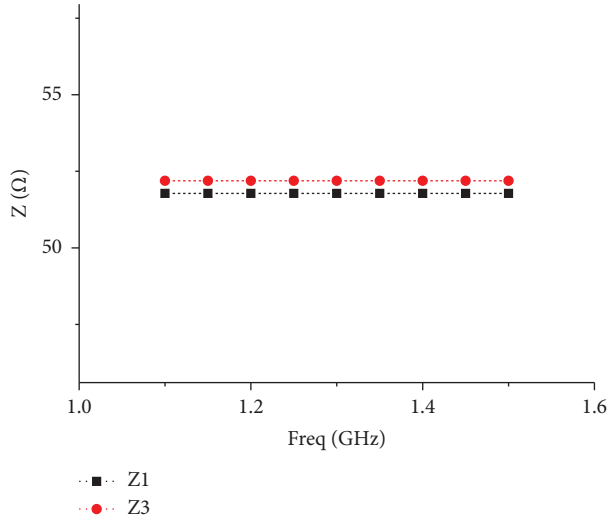

Figure 5: Impedance comparison of transmission lines.

$$K = \sqrt[3]{\left(\frac{Z_2'}{Z_3'}\right)^2}. \tag{7}$$

Or

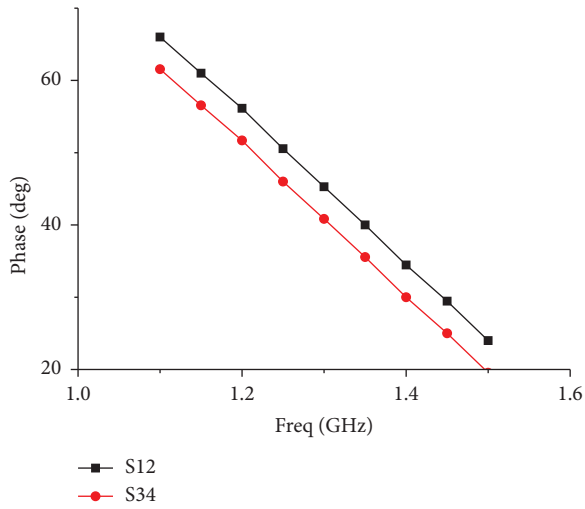

Figure 6: Phase comparison of transmission lines.

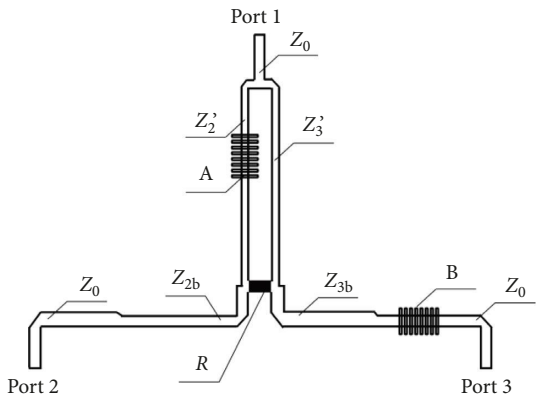

Figure 7: Integrated structure of an unequal power divider using louver-shaped DGS.

$$K = \frac{Z_{2b}}{Z_{3b}}. \tag{8}$$

If any of the impedance in Z_2', Z_3', Z_{2b} or Z_{3b} changes, the power ratio will change.

As shown in Figure 7, the transmission line has a characteristic impedance of 50 Ω, and the louver-shaped DGS is etched above the arm of the power divider. When the louver-shaped DGS is introduced at point A (above the arm of the power divider), the impedance (Z_2') of the circuit where the louver-shaped DGS is located increases, leading to a corresponding increase in phase. This results in a decrease in the output power of Port 2, as indicated by equation (7). Simultaneously, the output power of Port 3 increases. If the louver-shaped DGS is added at point B (above the 50 Ω transmission line), the phase of Port 3 also increases. By adding the louver-shaped DGS, the amplitude and phase relationship between Port 2 and Port 3 can be adjusted simultaneously.

Table 2: The design parameters of amplitude normalization.

Port	Normalized amplitude (dB)
1	−13.15
2	−10.75
3	−7.53
4	−4.88
5	−2.85
6	−1.41
7	−0.44
8	0
9	0
10	−0.44
11	−1.41
12	−2.85
13	−4.88
14	−7.53
15	−10.75
16	−13.15

5. Design and Measure of the Feeding Network

In order to obtain improved electrical performance characteristics of the feeding network, a novel 16-channel feeding network incorporating the louver-shaped DGS has been developed. The Taylor synthesis method, utilizing amplitude weighting, achieves a low sidelobe level of −32 dB in the design of this feeding network. Additionally, the phase consistency of each port is ensured. The design parameters for amplitude normalization of each port are detailed in Table 2. The design of the feeding network itself follows the general idea of weighted network design, which is not elaborated here.

Figure 8 shows a partial physical image of the feeding network. After the testing of the feeding network, the louver-shaped DGS corresponding to each port is adjusted based on the number of tests conducted. Because the processing tolerance of PCB itself has an impact on the power division ratio, it is impossible to predict the variation between the actual power ratio and the designed power ratio. In the circuit design, therefore, there is no provision for advanced configuration of the louver-shaped DGS for debugging power ratio. According to the test results, laser etching can be carried out on a large area above the impedance conversion section during later debugging. The pre-etched louver-shaped DGS for phase adjustment is positioned above the 50 Ω transmission line, near each port.

Debugging methods are as follows: A certain number of louver-shaped DGS are etched by laser at position A, as shown in Figure 7. Additionally, a certain number of the louver-shaped DGS are covered with copper foil or conductive silver paste at position B, also as shown in Figure 7. This procedure serves to decrease the amplitude of the port at position A and shorten the phase of the port at position B.

Figure 9(a) displays the test results for the amplitude deviation of central frequency before and after the debugging process. The difference between the measured value and the theoretical value has been zeroed at the eighth

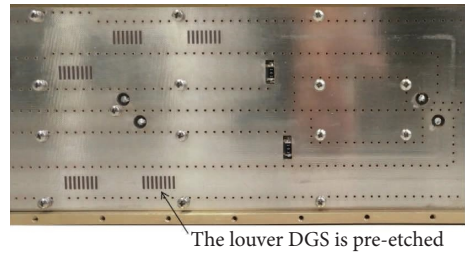

Figure 8: The part of a physical object.

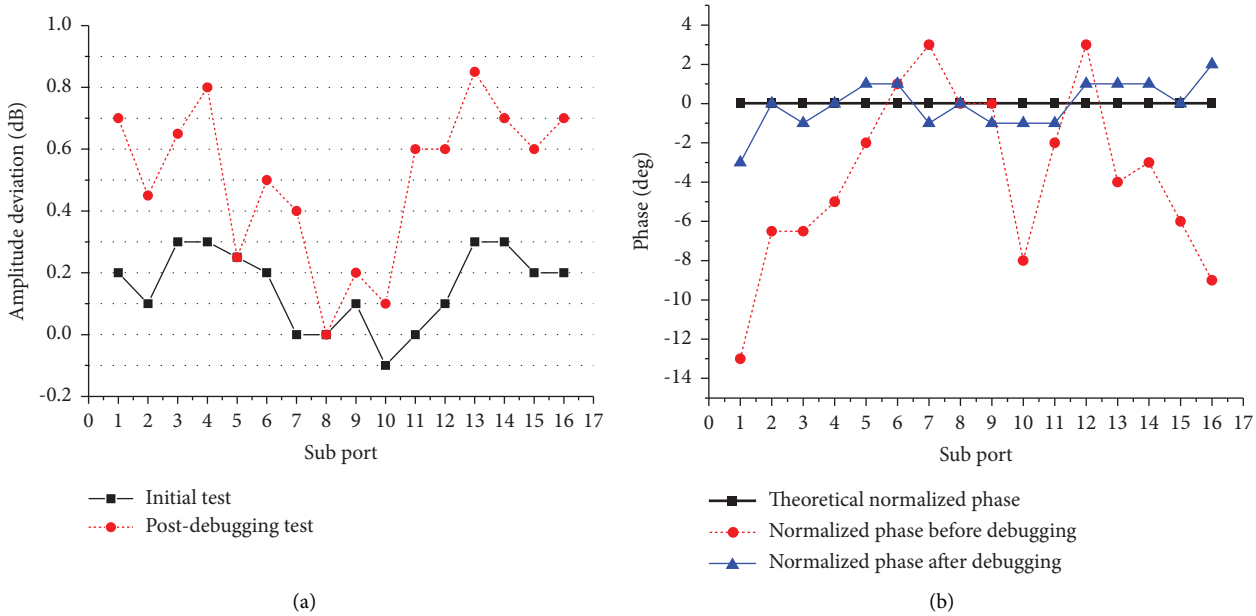

Figure 9: Test data before and after debugging for the central frequency points of the 16 sub-ports in the feeding network. (a) Amplitude deviation. (b) Phase deviation.

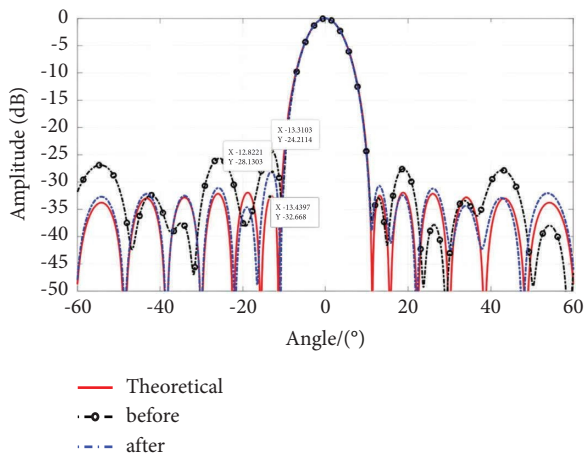

Figure 10: The directional pattern.

sub-port. Through the debugging procedure, the amplitude deviation of the feeding network is reduced from ±0.45 dB to ±0.2 dB.

Figure 9(b) displays the test results for the normalized phase of central frequency before and after the debugging process. All phases are zeroed at the eighth sub-port. Through debugging, the phase deviation of the feeding network has been reduced from ±8° before debugging to ±2.5° after debugging.

Figure 10 shows the pattern calculated from amplitude and phase data both before and after implementing the louver-shaped DGS for debugging. After debugging, the maximum value of the first sidelobe has been reduced from −24.2 dB to −28.1 dB.

The experimental results show that the performance of the line-feeding network is effectively improved by designing and adjusting the louver-shaped DGS.

6. Conclusions

In this paper, a low sidelobe feeding network has been developed utilizing the louver-shaped DGS. The louver-shaped DGS is positioned above the impedance conversion section of the power divider and the 50 Ω transmission line to adjust the amplitude and phase characteristics of each port within the feeding network.

The simulation test has demonstrated that after adding the louver-shaped DGS structure consisting of eight side-

by-side rectangular DGS units, the characteristic impedance of the stripline transmission line has increased by approximately 0.4 Ω at the center frequency (1.3 GHz), and the phase has lengthened by about 4.5° at the center frequency (1.3 GHz). In order to show the validity of the proposed DGS structure, the 16-channel feeding network incorporating the louver-shaped DGS has been designed, fabricated, and then measured. The test results indicate that the performance of the line-feeding network has been effectively improved by designing and adjusting the louver-shaped DGS. Through the debugging procedure, the amplitude deviation of the feeding network has been reduced from ±0.45 dB to ±0.2 dB, the phase deviation of the feeding network has been reduced from ±8° to ±2.5°, and the maximum value of the first sidelobe has been reduced from −24.2 dB to −28.1 dB.

By covering or increasing the louver-shaped DGS, the amplitude deviation and phase deviation of the feeding network are further reduced. This, in turn, improves the electrical performance of the feeding network greatly. This ensures that the final amplitude and phase align with the design specifications.

If there is a deviation between the actual production of the feeding network and the theoretical calculations, the feeding network may exhibit subpar performance during initial testing after trial production. Failure to debug it could render it essentially non-compliant. However, by adjusting the amplitude and phase of the feeding network through debugging the DGS, its performance can be enhanced to meet operational requirements, thereby obviating the need for re-production and significantly reducing production costs and lead times. This ensures that the final amplitude and phase meet the design requirements.

The adoption of this method can mitigate discrepancies between design and production process solidification, as well as material inconsistencies, thereby curtailing the need for iterative design and verification cycles and reducing production costs and lead times. Additionally, it reduces the requirements of material uniformity and processing technology of the feeding network, thereby improving the yield of the feeding network. This approach holds potential for the design of feeding networks for large strip array antennas and has been successfully implemented in the feeding network of large stripline array antennas, demonstrating exceptional performance in a radar product.

Data Availability

The data underlying this article will be shared on reasonable request to the corresponding author.

Conflicts of Interest

The authors declare that they have no conflicts of interest.

References

[1] E. Noh, Y. Kang, and K. Kim, "Slit-loaded series feeding network for millimeter-wave array antenna with a low sidelobe level over a wide bandwidth," *IEEE Transactions on Antennas and Propagation*, vol. 99, p. 1, 2020.

[2] A. Verma, R. K. Arya, R. Bhattacharya, and S. N. Raghava, "Compact PIFA antenna with high gain and low SAR using AMC for WLAN/C-band/5G applications," *IETE Journal of Research*, vol. 69, no. 7, pp. 4422–4432, 2023.

[3] C. Wang, Y. Wang, P. Lian et al., "Space phased array antenna developments: a perspective on structural design," *IEEE Aerospace and Electronic Systems Magazine*, vol. 35, no. 7, pp. 44–63, 2020.

[4] D. Zhang, Z. Zhou, and Z. Zhu, *Feed Technology of Radar*, Publishing House of Electronics Industry, Beijing, China, 2010.

[5] Y. W. Wu, Z. C. Hao, Z. W. Miao, W. Hong, and J. S. Hong, "A 140 Ghz high-efficiency slotted waveguide antenna using a low-loss feeding network," *IEEE Antennas and Wireless Propagation Letters*, vol. 19, no. 1, pp. 94–98, 2020.

[6] T. S. Mneesy, R. K. Hamad, A. I. Zaki, and W. A. E. Ali, "A novel high gain monopole antenna array for 60 Ghz millimeter-wave communications," *Applied Sciences*, vol. 10, no. 13, p. 4546, 2020.

[7] A. Verma and S. N. Raghava, "Circularly polarized hybrid mode substrate integrated waveguide antenna for two quadrant scanning beamforming applications for 5G," *International Journal of RF and Microwave Computer-Aided Engineering*, vol. 31, no. 10, Article ID 22798, 2021.

[8] T. V. Rao, A. Sudhakar, and K. P. Raju, "Novel technique of mimo antenna design for uwb applications using defective ground structures," *Journal of Scientific and Industrial Research*, vol. 77, no. 1, pp. 66–69, 2018.

[9] E. Jarauta and F. Falcone, "Stripline multilayer devices based on complementary split ring resonators," *Micromachines*, vol. 13, no. 8, p. 1190, 2022.

[10] S. Hang and Q. Li, "Design of a low sidelobe linear array," *Acoustics and Electronic Engineering*, vol. 4, pp. 14–16+23, 2022.

[11] S. Liu and C. Wang, "Low sidelobe reflector antenna design," *Computer Measurement & Control*, vol. 31, no. 6, pp. 246–251, 2023.

[12] H. Zhang, "A broadband low profile high gain low sidelobe array antenna," *Wireless Communication Technology*, vol. 32, no. 3, pp. 17–21, 2023.

[13] D. Duan, L. Hu, and Q. Guo, "Design of low sidelobe microstrip array antenna based on unequal power division ratio feed network," *Electronic Production*, vol. 30, no. 8, pp. 10–12+18, 2022.

[14] E. Yablonovitch, "Inhibited spontaneous emission in solid-state physics and electronics," *Physical Review Letters*, vol. 58, no. 20, pp. 2059–2062, 1987.

[15] J. I. Park, C. S. Kim, J. Kim et al., "Modeling of a photonic bandgap and its application for the low-pass filter design," in *Asia Pacific Microwave Conference Apmc99 Microwaves Enter the Century Conference*, IEEE, Singapore, November 2002.

[16] A. S. A. Nisha and T. Jayanthy, "Analysis of various parameters of square notch patch antenna using energy band gap and defected ground structure," *International Journal of Microwave and Optical Technology*, vol. 6, no. 5, pp. 271–277, 2011.

[17] K. Suvarna, N. R. Murty, and D. V. Vardhan, "A miniature rectangular patch antenna using defected ground structure for wlan applications," *Progress in Electromagnetics Research C*, vol. 95, pp. 131–140, 2019.

[18] A. Ghaloua, J. Zbitou, J. Zbitou, M. Latrach, A. Tajmouati, and A. Errkik, "A novel configuration of a miniature printed antenna array based on defected ground structure,"

International Journal of Intelligent Engineering and Systems, vol. 12, no. 1, pp. 211–220, 2019.

[19] F. Li, *Design and Research of Microstrip Filter Based on DGS*, Nanjing University of Posts and Telecommunications, Nanjing, China, 2018.

[20] D. J. Woo and T. K. Lee, "An equivalent circuit model for a dumbbell-shaped DGS microstrip line," *Journal of electromagnetic engineering and science*, vol. 14, no. 4, pp. 415–418, 2014.

[21] X. Song-tao and W. Xiao-po, "A serial feeding network with defected ground structure," *Journal of Radars*, vol. 3, no. 3, pp. 295–230, 2014.